

# Comptonization and reflection of X-ray radiation and the X-ray-radio correlation in the $\chi$ -states of GRS 1915+105<sup>★</sup>

A. Rau<sup>1,2</sup> and J. Greiner<sup>1,2</sup>

<sup>1</sup> Astrophysical Institute Potsdam, An der Sternwarte 16, 14482 Potsdam, Germany

<sup>2</sup> Max-Planck-Institute for extraterrestrial Physics, Giessenbachstrasse, 85748 Garching, Germany

Received 8 March 2002 / Accepted 31 May 2002

**Abstract.** We present a comprehensive X-ray study of four years of pointed *RXTE* observations of GRS 1915+105 in the  $\chi$ -state. We interpret the behavior of the hard power law tail spectrum as coming from inverse Compton scattering of soft disk photons on a thermally dominated hybrid corona above the accretion disk. GRS 1915+105 shows a strong, variable reflection amplitude. As in other BHC and in Seyfert galaxies, a correlation between the power law slope and the reflection was found. Also, the radio fluxes at 2.25 GHz and 15 GHz correlate with the power law slope, thus revealing a connection between the outflowing matter and the comptonizing region in the  $\chi$ -states.

**Key words.** X-rays: stars – stars: binaries: close – X-rays: individual: GRS 1915+105

## 1. Introduction

With the discovery of superluminal ejections (Mirabel & Rodriguez 1994) from the galactic transient source GRS 1915+105 and GRO J1655-40, much observational and theoretical attention has been directed to the field of microquasars. Microquasars are thought to be downscaled analogs to quasars exhibiting much smaller time scales and are therefore potential laboratories for studying accretion and relativistic jets near black holes (Mirabel et al. 1992). The most prominent object of this type is the galactic X-ray binary system GRS 1915+105 which shows dramatic variability (Greiner et al. 1996) in light curve, quasi-periodic oscillations, phase lags and coherence behavior (Morgan et al. 1997; Munro et al. 2001). GRS 1915+105 is the most energetic object known in our galaxy with a luminosity of  $\sim 10^{38}$  erg/s in the low state.

GRS 1915+105 harbors a black hole of  $14 M_{\odot}$  (Greiner et al. 2001b) making it the most massive stellar black hole known. Being in the galactic plane and at a distance of  $\sim 12$  kpc the source suffers a very high extinction in the optical band of the order of 25–30 mag (Greiner et al. 1994; Chaty et al. 1996). Greiner et al. (2001a) found the donor to be an K–M III late type giant as determined from absorption line measurements in the near infrared.

Black hole transients generally exhibit different states of intensity and spectrum: the high/soft state with a prominent disk

component and a weak or negligible steep power law tail, the low/hard state with negligible accretion disk and flat power law. In the intermediate and very high state both the accretion disk and a power law are seen.

Originally discovered by *Granat* (Castro-Tirado et al. 1992), GRS 1915+105 was extensively monitored by the *RXTE* since 1996 and a number of investigations of these data have been published (e.g. Morgan et al. 1997; Belloni et al. 1997, 2000; Munro et al. 1999, 2000).

The source evades simple classification, although it seems to spend most of the time in the very high state. Several attempts to categorize the behavior of GRS 1915+105 have been made in the past. Belloni et al. (2000) defined 12 different states depending on light curve variation and hardness colors. One of these states, the so-called  $\chi$ -state is characterized by a lack of obvious variations in the light curve and spectrum and is associated with continuous radio emission of differing strength.  $\chi$ -states correspond to the low/hard state of GRS 1915+105, exhibiting relatively low flux from the accretion disk and showing a hard power law tail. These states resemble long variants of the lulls in  $\beta$ -states, when part of the inner accretion disk is proposed to be absent. Depending on the strength of the radio emission, differing phase lag and power spectrum behavior are seen. During the so-called radio quiet  $\chi$ -states the phase lag of the hard X-ray photons to the soft X-ray photons is partly negative, whereas it is always positive when the radio emission is strong (Munro et al. 2001). Also, the frequency of the 0.5–10 Hz QPO decreases with increasing radio flux.

In this paper we present a comprehensive study of the X-ray spectral behavior of GRS 1915+105 in the  $\chi$ -state with over nearly four years of observation with *RXTE*.

Send offprint requests to: A. Rau, e-mail: arau@xray.mpe.mpg.de

<sup>★</sup> Complete Table 2 is only available in electronic form at the CDS via anonymous ftp to cdsarc.u-strasbg.fr (130.79.128.5) or via

<http://cdsweb.u-strasbg.fr/cgi-bin/qcat?J/A+A/397/711>

The variation of the spectral properties is then compared to those of the radio emission. Valuable information about the disk geometry and properties of the compact object is derived.

## 2. Data selection and analysis

### 2.1. *RXTE*

For our investigation of GRS 1915+105 we used public *RXTE* data from November 1996 to September 2000 provided by HEASARC. We selected Proportional Counter Array (PCA) and High Energy X-Ray Timing Experiment (HEXTE) data of 139  $\chi$ -state observations from 89 different days. The selection of the datasets was based on the  $\chi$ -states defined by Belloni et al. (2000) and on PCA light curves provided by E. H. Morgan<sup>1</sup>. Data with more than 30 min away from the South Atlantic Anomaly and without X1908+075 in the HEXTE background<sup>2</sup> were selected. The lack of obvious variability in the light curve and its spectral hardness allows long continuous exposure times and therefore high signal-to-noise ratios. Typically, the spectra during this state show blackbody emission arising from an accretion disk and a dominating power law hard energy tail.

We reduced the *RXTE* data using the standard reduction script REX included in the HEASoft5.04 package. We restricted the analysis to Standard 2 binned data of all layers of PCU0 of the PCA from 3–25 keV and HEXTE cluster 0 from 20–190 keV only. We used PCARSP 7.10 to produce a particular response matrix for each PCU0 dataset. In order to account for part of the uncertainties in the PCU0 instrument we added a systematic error of 1% as recommended (Remillard<sup>3</sup>).

The X-ray spectral fitting was done using XSPEC 11.0 (Arnaud 1996). A consistent model should fit all *RXTE*  $\chi$ -state data. Therefore we tested several X-ray radiation models and finally selected a model consisting of (i) photoelectric absorption (WABS; Balucinska-Church & McGammon 1992), (ii) a spectrum from an accretion disk consisting of multiple blackbody components (DISKBB) and (iii) a power law spectrum reflected from an ionized relativistic accretion disk (REFSCH; Fabian et al. 1989; Magdziarz & Zdziarski 1995). Several attempts in the past to fit GRS 1915+105 spectra have shown complicated residuals in the soft X-ray band suggesting the existence of emission and/or absorption features near 6.4 keV, the energy of the Fe K $\alpha$  line (Kotani et al. 2000). Because of the low spectral resolution of  $\sim 1$  keV of the PCA at this energy an additional line fit gives no meaningful results. Therefore we ignored all energy bins from 4.5 to 8.5 keV while fitting our model. We fixed the hydrogen column density at  $N_{\text{H}} = 5 \times 10^{22} \text{ cm}^{-2}$  as determined by Greiner et al. (1994) with *ROSAT*. It has been shown that the disk blackbody + power law assumption strongly overestimates the flux at lower energies compared to the thermal and non-thermal comptonization models used by Vilhu et al. (2001) and Zdziarski et al. (2001), respectively. This explains the smaller  $N_{\text{H}}$  ( $2\text{--}3 \times 10^{22} \text{ cm}^{-2}$ ) values they found for  $\chi$ -state observations. However, because

**Table 1.** Fixed parameters of the spectral model.

fix. parameter	value
$N_{\text{H}}$	$5 \times 10^{22} \text{ cm}^{-2}$
cutoff energy	no cutoff
redshift	0
$Z > 2$ element abundances	1
iron abundance to abundance above	1
inclination angle	$70^\circ$
power law index for reflection emissivity	-2
inner disk radius	$6 \text{ GM}/c^2$
outer disk radius	$1000 \text{ GM}/c^2$

we ignored the energy bins from 4.5 to 8.5 keV the amount of data bins needed to adjust the hydrogen column density was too small to let  $N_{\text{H}}$  be a free parameter.

We fixed 9 of the combined 16 model parameters (Table 1), leaving free the accretion disk temperature,  $T_{\text{bb}}$ , and relative normalization,  $K_{\text{bb}} \propto R_{\text{in}}^2$ , the power law photon index,  $\Gamma$ , with  $N \propto E^{-\Gamma}$  and relative normalization,  $K_{\text{po}}$  (photons/keV/cm<sup>2</sup>/s at 1 keV), the reflection index,  $R$ , the ionization parameter,  $\xi$ , and a factor to account for the relative normalization between PCU0 and HEXTE cluster 0. If not stated otherwise, we plot  $1\sigma$  errors for each parameter of interest.

### 2.2. *GBI* and *RT*

The appearance of steady radio emission in  $\chi$ -states suggested us to search for correlations between *RXTE* data and radio data at 15 GHz (*Ryle Telescope* = *RT*) and 2.25 GHz (*Green Bank Interferometer* = *GBI*). GRS 1915+105 shows variability at all frequencies on time scales of seconds to hours. For a useful statement in  $\chi$ -states a suitable selection of corresponding datasets is therefore required.

According to the general interpretation that the radio emission is synchrotron emission from ejected plasma in sporadic or continuous jets (Fender et al. 1995) the radio flux should reach a maximum 15 min after the actual ejection (Mirabel et al. 1997) and therefore after a possible determining X-ray event.

Figure 1 shows the 15 GHz radio flux,  $F_{\text{R}}$ , from the *RT* for JD 2450898–2450913 together with two *RXTE* observations. The *RT* observed GRS 1915+105 several times a day with five minute exposures.

Because the radio exposure is much shorter than the X-ray exposure ( $\sim$ hour) it is important to select radio data simultaneous with the *RXTE* observations. 37 of the 139 analyzed *RXTE* observations have simultaneous *RT* data and 9 have simultaneous *GBI* data.

Still, the selection of simultaneous radio observations is non-trivial. Occasionally the radio emission varies also during a single  $\chi$ -state X-ray observation, whereas no variability is seen in X-ray count rate and hardness ratio (5.2–60 keV/2–5.2 keV) (Fig. 2). But the variation of  $F_{\text{R}}$  during a  $\chi$ -state observation is negligible compared to the uncertainties of the individual radio measurements and to the variation between different *RXTE* observations. Therefore, the radio fluxes were averaged for each *RXTE* observation.

<sup>1</sup> [http://xte.mit.edu/~ehm/1915\\_frames.html](http://xte.mit.edu/~ehm/1915_frames.html)

<sup>2</sup> <http://mamacass.ucsd.edu:8080/cgi-bin/HEXTEROCK.html>

<sup>3</sup> <http://lheawww.gsfc.nasa.gov/users/keith/ronr.txt>

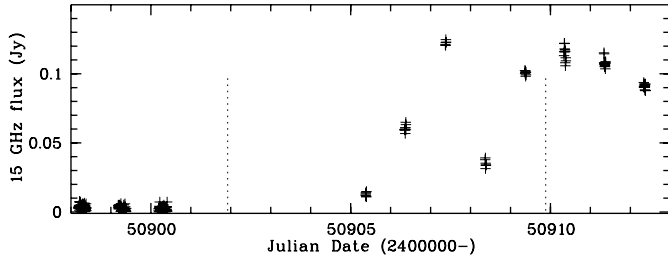


**Fig. 1.** Variation of the 15 GHz flux (crosses) between JD 2450898 and JD 2450913. The dotted lines mark the time of *RXTE* observations from 29.03.1998 (JD  $\sim$  2450902) and 06.04.1998 (JD  $\sim$  2450910). GRS 1915+105 showed low radio emission until JD 2450900.5. The source was dominated by strong, variable radio emission following JD 2450905. No statement can be made about the time in between, because of the lack of radio observations during the *RXTE* observation from 29.03.1998. Also for the *RXTE* observation from 06.04.1998 the radio flux is uncertain because of the strong variation before and after the X-ray exposure.

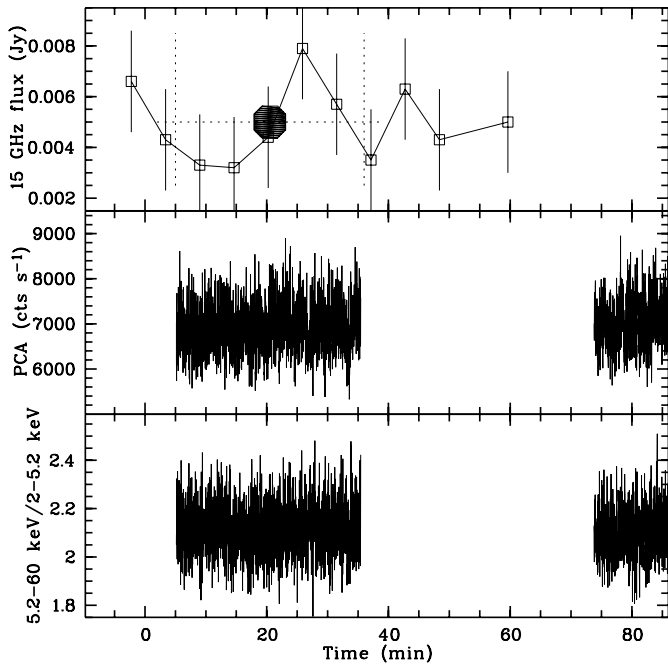


**Fig. 2.** 15 GHz light curve (*RT*, upper panel), 2–60 keV PCA light curve (middle panel) and hardness ratio  $\frac{5.2-60 \text{ keV}}{2-5.2 \text{ keV}}$  (lower panel) of the  $\chi$ -state from 15.09.1998 (JD 2451071.9). While the radio light curve shows structured variability, none is seen in X-ray intensity and spectrum. The large black dot (marked for clarity with the dotted lines) in the upper panel represents the averaged radio flux over the *RXTE* observation used for further analysis.

### 3. Results of the analysis

The spectra of all 139 datasets have been fitted with the above-described DISKBB+REFSCH model. Two example model spectra are shown in Fig. 3. These spectra have the extreme values of  $\Gamma$  and  $R$ , revealing the spectral differences between different  $\chi$ -state observations.

The best fit parameters for the  $\chi$ -states of GRS 1915+105 are shown in Fig. 4 and Table 2, respectively. The upper two panels in Fig. 4 show the strong variability of the source in

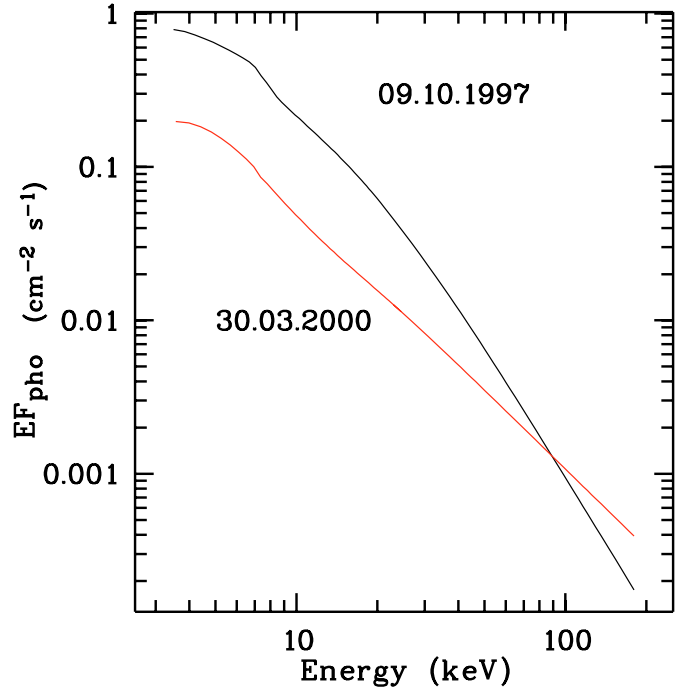


**Fig. 3.** Combined PCU0 and HEXTE cluster 0 spectra of the  $\chi$ -states from 09.10.1997 (down, artificially offset for better discrimination) and 30.03.2000 (top). These spectra show extreme power law slope ( $\Gamma = 3.41 \pm 0.06$  (09.10.1997),  $\Gamma = 2.65 \pm 0.05$  (30.03.2000) and reflection ( $R = 7.43 \pm 1.12$  (09.10.1997),  $R = 0.35 \pm 0.23$  (30.03.2000) behavior. Note the obvious reflection hump for the 09.10.1997 spectra at  $\sim$ 10 keV.

the 1.5–12 keV (*RXTE* All Sky Monitor (ASM)) and 2.25 GHz (*GBI*) bands from JD 2450300–2451900. Irregular outburst and relatively quiet phases alternate in X-ray and radio without any obvious coupling.

The lower six panels of Fig. 4 show the PCU0 count rate and the fit parameters of the  $\chi$ -state observations. The red and black data points mark two groups of observations with different  $\Gamma(K_{\text{po}})$  behavior (see Fig. 5).

Between the  $\chi$ -states, the PCU0 count rate varies, with some exceptions, by a factor of 2 at most. Only during the long continuous  $\chi$ -state at JD  $\sim$  2450400–2450600 and at JD  $\sim$ 2451750 recurrent variability in the X-ray count rate is observed. The model parameters of DISKBB+REFSCH are variable. The power law slope,  $\Gamma$ , varies between 2.4 and 3.5 with a long-term periodicity of  $\sim$ 590 days (Rau & Greiner 2002, in preparation). No correlation of  $\Gamma$  and PCU0 count rate is seen, except around JD  $\sim$  2450500 and JD  $\sim$  2451750. The power law normalization behaves similarly to the slope.

The reflection component,  $R$ , is variable between different  $\chi$ -state observations and shows a long-term variability similar to the power law slope. It varies between 0 and 10 (upper limit of our model) with rather large uncertainties when  $R > 4$ . Except for five observations when  $R < 1$ , this rules out an isotropically sandwiching corona above the entire accretion disk.

The significance of the accretion disk component varies through the  $\chi$ -states. For some observations the disk is more or less absent (e.g. JD 50400–50600; relatively low disk

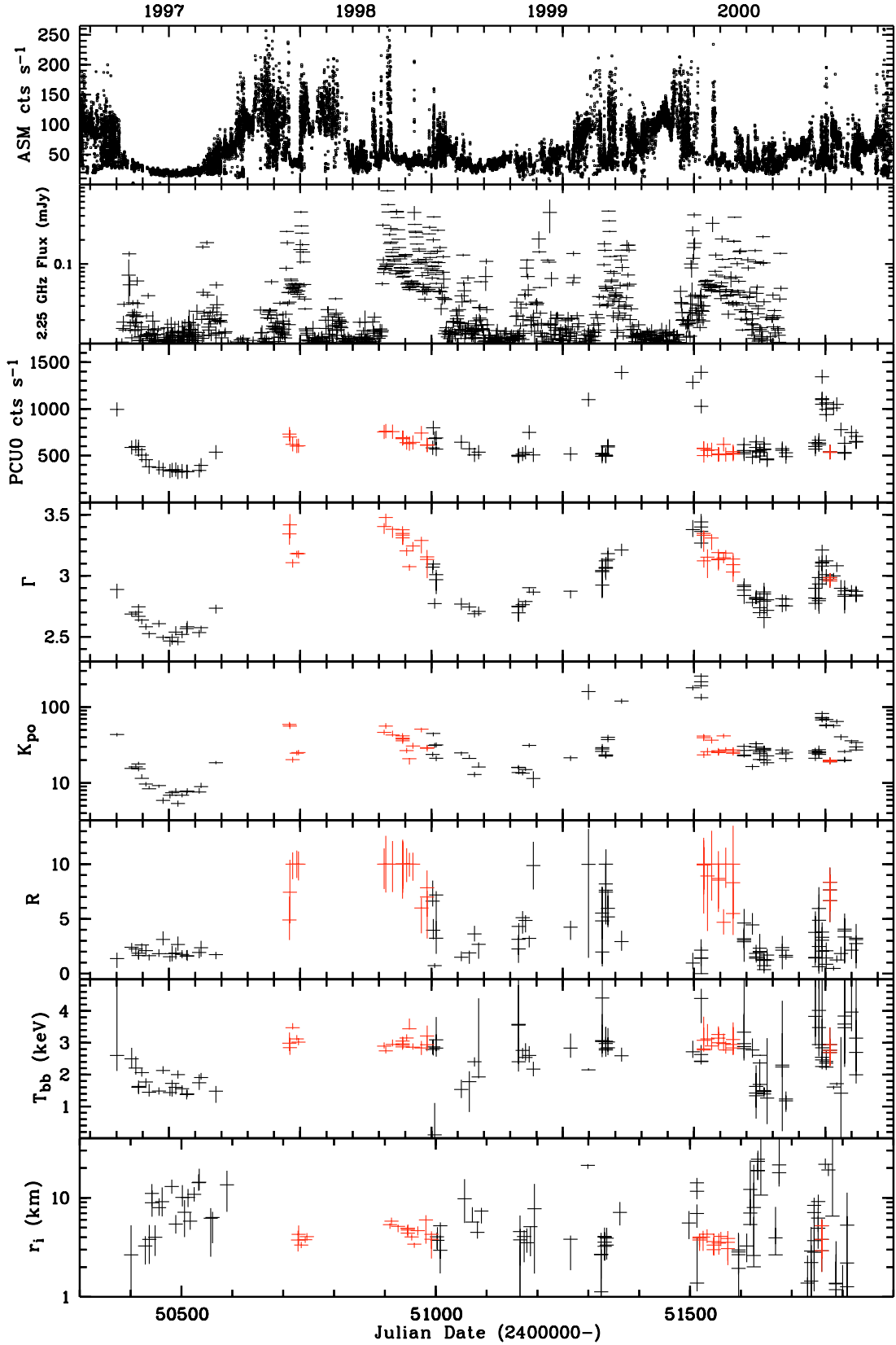


**Fig. 4.** 1.5–12 keV ASM count rate (1st panel from top) and 2.25 GHz *GBI* flux (2nd) from November 1996 to September 2000. (*GBI* was off-line some time before JD  $\sim$  2450400 and following JD  $\sim$  2451660. The lower panels show the 3–20 keV PCU0 count rate (3rd), the power law slope,  $\Gamma$ , (4th) and power law normalization,  $K_{po}$ , (5th), the reflection amplitude,  $R$ , (6th), the accretion disk temperature,  $T_{bb}$ , (7th) and the inner disk radius (determined from the disk normalization),  $r_i$ , (8th) for all analysed  $\chi$ -states of GRS 1915+105. Error bars are  $1\sigma$  for one parameter of interest. The observations of the two different branches in the  $\Gamma(K_{po})$  behavior are marked with red (steep) and black (flat) as in Fig. 5.

**Table 2.** Fit results of the *RXTE* spectra using the DISKBB+REFSCH model (The complete table is available at CDS). (1): ID of observation ( $I = 10402-01$ ,  $J = 20187-02$ ,  $K = 20402-01$ ,  $L = 30182-01$ ,  $M = 30402-01$ ,  $N = 30703-01$ ,  $O = 40703-01$ ,  $P = 50703-01$ ), (2): exposure time of observation, (3): 3–20 keV PCU0 count rate, (4): 20–190 keV HEXTE cluster 0 count rate, (5): accretion disk temperature, (6): accretion disk normalization ( $K_{bb} = (\frac{r}{D/10 \text{ kpc}})^2 \cos \theta$ ), (7): power law slope, (8): reflection amplitude, (9): power law normalization (photons/keV/cm<sup>2</sup>/s at 1 keV), (10): ionization parameter, (11): factor for normalization of PCU0 and HEXTE cluster 0, (12): reduced  $\chi^2$ . All errors are  $1\sigma$  for each parameter of interest.

Obs-ID <sup>(1)</sup>	GD	JD (-2400000)	Exposure <sup>(2)</sup> [s]	PCU0 <sup>(3)</sup> [cts/s]	HEXTE0 <sup>(4)</sup> [cts/s]	$T_{bb}$ <sup>(5)</sup> [keV]	$K_{bb}$ <sup>(6)</sup>	$\Gamma$ <sup>(7)</sup>	$R$ <sup>(8)</sup>
K-02-01	14.11.1996	50401.12	2688	995	70	2.60 <sup>+4.81</sup> <sub>-0.49</sub>	1.67 <sup>+4.90</sup> <sub>-1.60</sub>	2.89 <sup>+0.05</sup> <sub>-0.07</sub>	1.37 <sup>+0.55</sup> <sub>-0.86</sub>
K-06-00	11.12.1996	50428.86	8656	587	60	2.50 <sup>+0.35</sup> <sub>-0.30</sub>	2.52 <sup>+1.46</sup> <sub>-1.45</sub>	2.69 <sup>+0.02</sup> <sub>-0.02</sub>	2.40 <sup>+0.40</sup> <sub>-0.44</sub>
K-07-00	19.12.1996	50436.74	8992	598	61	2.21 <sup>+0.36</sup> <sub>-0.21</sub>	3.42 <sup>+3.25</sup> <sub>-2.32</sub>	2.70 <sup>+0.01</sup> <sub>-0.03</sub>	2.25 <sup>+0.20</sup> <sub>-0.56</sub>
.	.	.	.	.	.	.	.	.	.
P-28-00	21.09.2000	51808.70	2384	706	69	2.70 <sup>+1.39</sup> <sub>-0.73</sub>	1.14 <sup>+8.85</sup> <sub>-1.01</sub>	2.84 <sup>+0.03</sup> <sub>-0.06</sub>	3.11 <sup>+1.42</sup> <sub>-2.64</sub>
P-28-01	21.09.2000	51808.77	2400	651	66	3.15 <sup>+3.59</sup> <sub>-1.05</sub>	0.38 <sup>+0.21</sup> <sub>-0.37</sub>	2.83 <sup>+0.08</sup> <sub>-0.04</sub>	2.74 <sup>+0.22</sup> <sub>-1.29</sub>
P-28-02	21.09.2000	51808.83	2336	645	44	2.00 <sup>+1.72</sup> <sub>-0.28</sub>	6.65 <sup>+23.43</sup> <sub>-6.47</sub>	2.87 <sup>+0.05</sup> <sub>-0.03</sub>	3.24 <sup>+0.24</sup> <sub>-2.29</sub>

Obs-ID	$K_{po}$ <sup>(9)</sup> [Pho/keV/cm <sup>2</sup> /s]	$\xi$ <sup>(10)</sup>	$c$ <sup>(11)</sup>	$\chi^2$ <sup>(12)</sup>
K-02-01	43.5 <sup>+2.0</sup> <sub>-2.6</sub>	4999 <sup>+1</sup> <sub>-3521</sub>	0.82	0.69
K-06-00	15.6 <sup>+1.2</sup> <sub>-0.3</sub>	5000 <sup>+0</sup> <sub>-4421</sub>	0.78	1.00
K-07-00	16.3 <sup>+1.1</sup> <sub>-0.4</sub>	996 <sup>+4004</sup> <sub>-338</sub>	0.79	1.01
.	.	.	.	.
P-28-00	34.1 <sup>+0.7</sup> <sub>-5.0</sub>	2902 <sup>+2098</sup> <sub>-2902</sub>	0.82	0.94
P-28-01	29.8 <sup>+0.1</sup> <sub>-2.1</sub>	462 <sup>+4538</sup> <sub>-461</sub>	0.81	0.84
P-28-02	27.2 <sup>+2.8</sup> <sub>-0.8</sub>	34 <sup>+2900</sup> <sub>-34</sub>	0.52	0.77

temperature and large inner disk radius (small normalization)), for other observations the disk component provides a non-negligible contribution to the X-ray flux (e.g. JD 51500–51600; high temperature and small inner radius). In order to be consistent and to fit all  $\chi$ -state observations with the same model, we included the DISKBB component in all of our fits, although it could be excluded for several observations.

The accretion disk component shows a variable disk temperature of 1–4 keV. Sometimes, large uncertainties due to the small contribution of the DISKBB component to the total flux are seen. The inner disk radius, which can be determined from the disk normalization, varies between 1 and 20 km. For a non-rotating black hole of mass  $14 M_{\odot}$  (as measured for GRS 1915+105, Greiner et al. 2001b) the Schwarzschild radius is  $\sim 40$  km. It is known that the DISKBB model underestimates the inner disk radius by a factor of 1.7–3 due to Doppler blurring and gravitational redshift (Merloni et al. 2000). Also the neglect of comptonization in the surface layers of the disk leads to unphysical values when using then DISKBB model (Zdziarski et al. 2001). But even a maximally rotating black hole (where the inner disk radius reaches the Schwarzschild radius) cannot account for the majority of the parameter values. This problem has to be kept in mind when discussing the absolute values of the parameters.

Another free physical parameter of the REFSCHE model is the ionization parameter,  $\xi$ . It has huge uncertainties because no Fe  $K\alpha$  line could be fitted but has a negligible influence on the hard X-ray continuum and our model parameters. Therefore

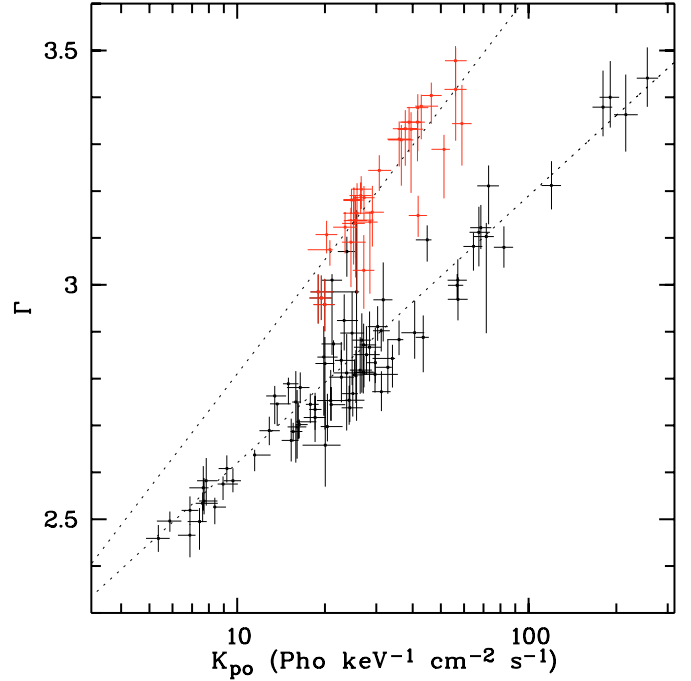


**Fig. 5.** Power law slope,  $\Gamma$ , as a function of power law normalization,  $K_{po}$ . Each *RXTE* observation is represented by one data point. The upper branch presents the red points in Fig. 4 and the lower branch the black points, respectively. The dotted lines represent the fitted correlation functions (see text).

we will not plot or discuss  $\xi$  further. Theoretically, the reflection in the hard spectrum should depend on the ionization parameter because higher ionization means lower absorption and therefore higher reflection probability. But the REFSCHE model includes a simple 1-ionization zone model only, which is very unlikely to be present in the disk and does not show any dependence of reflection and ionization at all.

### 3.1. The power law component

The model fits reveal an increasing power law normalization,  $K_{po}$ , with a steepening power law component (Fig. 5)

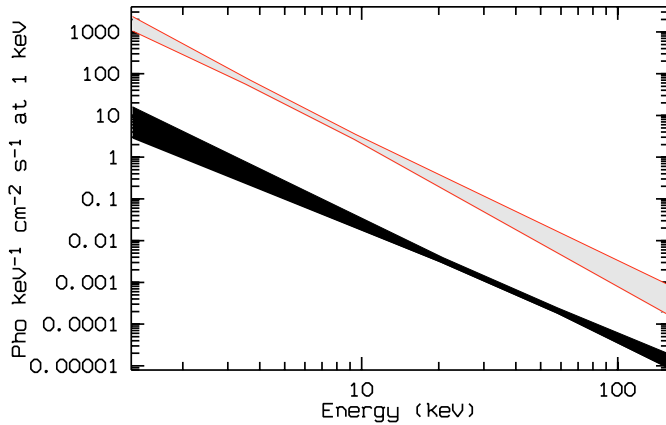


**Fig. 6.** Schematic power law spectra for the upper (top) and lower (bottom) branch of Fig. 5, the red and black points from Fig. 4, respectively, artificially offset by a factor of 100. The pivoting happens at different energies (4–8 keV & 20–30 keV).

suggesting a pivoting behavior. Two branches with different slopes are seen in the correlation. No correlation of the power law slope with the X-ray count rate in ASM and/or PCU is observed.

The strength of the correlation can be tested using a Spearman rank-order correlation test (Press et al. 1992). Both branches show strong correlations (steeper:  $r_s = 0.85$ , flatter:  $r_s = 0.87$ ). (Note, this statistical method does not take into account the particular uncertainties of the data points.)

The best descriptions of the correlations are functions of the type

$$\Gamma = u \cdot \log K + v \quad (1)$$

with  $u = 0.57 \pm 0.02$  and  $v = 2.0 \pm 0.1$  for the lower branch and  $u = 0.81 \pm 0.07$  and  $v = 2.0 \pm 0.1$  for the upper branch.

The pivoting has been tested in more detail by schematically plotting the obtained power law spectra. The two different branches consequently show different pivoting behavior (Fig. 6). Whereas the upper branch from Fig. 5 shows a pivoting energy of 4–8 keV (gray), the lower branch pivots at around 20–30 keV (black).

### 3.2. Reflection

Due to the known uncertainties of the PCA below 6 keV (Jahoda et al. 1996) and the low energy resolution, stringent conclusions about the behavior of an iron line in the *RXTE* spectra at 6.4–7 keV not can be drawn. For the analysis of the reflection, therefore, only the continuum radiation can be used, manifesting itself in the reflection hump from 10–30 keV.

The reflection amplitude in GRS 1915+105 as a function of  $\Gamma$  is shown in Fig. 7 together with that of three black hole candidates (Cyg X-1, GX 339-4 and GS 1354-644; Gilfanov et al. 2000). Although  $R$  shows large uncertainties for the  $\chi$ -states of GRS 1915+105, a similar correlation is seen as in the other X-ray binaries. The steeper the power law component, the higher is the reflected fraction of photons. Figure 7 contains the confidence intervals of  $R$  for three observations to clarify the influence of the model on the  $R(\Gamma)$ -correlation.

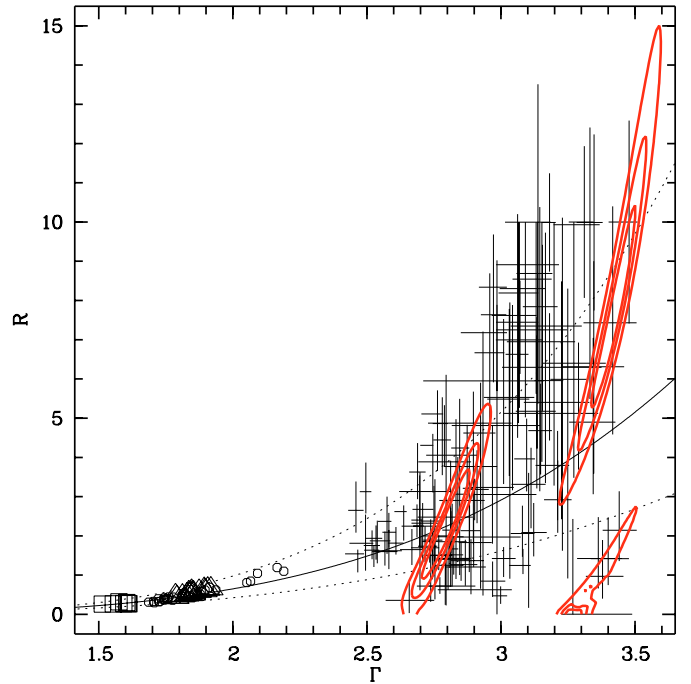


**Fig. 7.**  $R(\Gamma)$ -correlation for GRS 1915+105 (crosses) and three X-ray binaries (Cyg X-1 = circles, GX 339-4 = triangles and GS 1354-644 = squares; from Gilfanov et al. 2000). The solid line represents the best fitting model function and the dotted lines the upper and lower limits. Overplotted are the 1, 2 and 3  $\sigma$  confidence contours for three different observations (from left: N-23-01, K-49-01, O-40-03). Note the data points (JD 2451497–2451513) at  $\Gamma \sim 3.3$ –3.5 and  $R \sim 0$ –2 behaving remarkably different.

Although the contours are elongated similar to the correlation (higher  $\Gamma$  has higher  $R$ ), they are intrinsically steeper compared to the overall correlation. Thus, the existence of the  $R(\Gamma)$ -correlation in the  $\chi$ -states of GRS 1915+105 is no artifact of the model.

A group of observations at high  $\Gamma$  (3.3–3.5) and small  $R$  (0–2) behaves remarkably differently. These points belong to five datasets from JD 2451497 and JD 2451513 showing very high PCU0 count rates (1300–2100 cts/s) and are short duration  $\chi$ -states between different high variability states.

The correlation of  $R$  and  $\Gamma$  is tested using a Spearman rank-order correlation test. The correlation is distinct ( $r_s = 0.61$ ) but not strong.

For a quantitative description of the correlation, a phenomenological function was fitted to the data. The best-fitting model is a power law

$$R = u \cdot \Gamma^v, \quad (2)$$

with  $u = 0.05 \pm 0.007$  and  $v = 3.7 \pm 0.4$  (solid line in Fig. 7).

### 3.3. X-ray-radio-correlation

No obvious correlation between the soft X-ray component and the radio emission is seen. Neither the soft X-ray flux, the temperature of the accretion disk nor the inner disk radius show a correlation with the 15 GHz radio flux from *RT* and/or *GBI*.

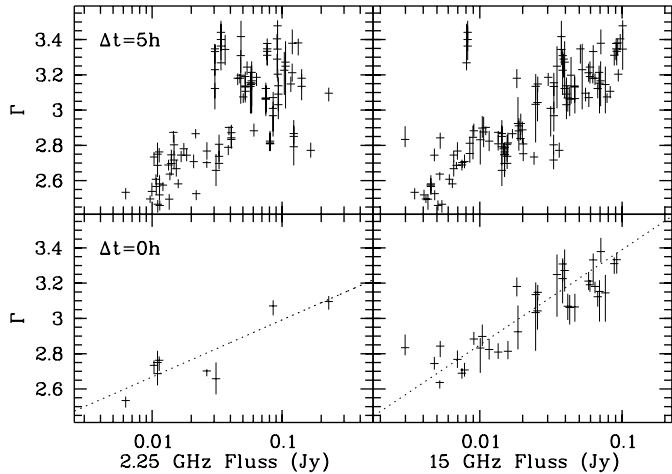


**Fig. 8.**  $\Gamma(F_R)$ -correlation for *GBI* (left) and *RT* (right). Upper panels: correlation for  $\Delta t = 5$  hrs (time between *RXTE* and radio observation). As for *GBI* and for *RT* the correlation is visible but the data points show a large spread. Lower panel: correlation for  $\Delta t = 0$  hrs. The dotted lines represent the correlation functions.

An unexpected result is found when plotting  $\Gamma$  vs.  $F_R$  (Fig. 8). The power law slope correlates positively with the radio flux at 2.25 GHz and 15 GHz. Observations with high radio emission show a softer X-ray spectrum (steeper power law component). Note that no bimodality in the radio emission exists. Instead, a continuous spread is observed. A strict separation of radio loud and radio quiet  $\chi$ -states, as done before (e.g. Muno et al. 2001; Trudolyubov 2001) seems therefore unsubstantiated.

The correlation of  $\Gamma$  and  $F_R$  is most obvious for simultaneous ( $\Delta t = 0$  hrs) observations. Datasets with radio observations  $\pm 5$  hrs offset also show the correlation (Fig. 8 upper panel) but with significant scattering. Usually, no statement about the variability state before and after the *RXTE* exposure can be made, because the source may have had several state alterations. Thus, non-simultaneity is the likely reason for the strong scattering of the correlation for  $\Delta t = 5$  hrs in comparison to  $\Delta t = 0$  hrs.

To determine the strength of the correlation a Spearman rank-order correlation test was made for the *RT* data with  $\Delta t = 0$  h. The correlation is strong ( $r_s = 0.83$ ). No test was made for *GBI* due to the small number of simultaneous *GBI/RXTE* datasets.

The next step was to fit a phenomenological function (dotted line in Fig. 8) to the correlation. The best model functions are of the form

$$\Gamma = u \cdot \log F_R + v, \quad (3)$$

with  $u = 0.54 \pm 0.02$  and  $v = 3.94 \pm 0.03$  for *RT* and  $u = 0.32 \pm 0.05$  and  $v = 3.3 \pm 0.1$  using *GBI* data.

Besides the  $F_R(\Gamma)$ -correlation we also investigated the relation between  $F_R$  and the X-ray flux of the power law component. This introduces some freedom as to at which lower energy the power law is “chosen”. Figure 9 shows the X-ray flux from 20–200 keV and 1–200 keV, respectively, over the radio flux.

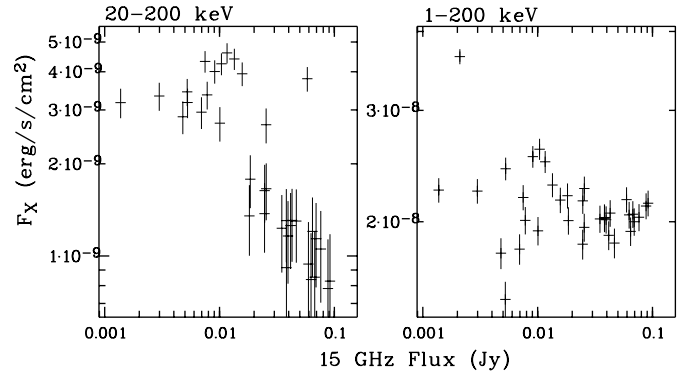


**Fig. 9.** 20–200 keV (left) and 1–200 keV (right) X-ray flux shown over the 15 GHz radio flux (*RT*). The 20–200 keV flux has a negative correlation with the radio flux, whereas the 1–200 keV flux does not show such a correlation.

**Table 3.** Observed correlation of the  $\chi$ -states of GRS 1915+105.

correlation between:	type <sup>(1)</sup>	ref.
$\Gamma$	$K_{po}$	+
$\Gamma$	$F_R$	+
$\Gamma$	$R$	+
$F_X(20\text{--}200 \text{ keV})$	$F_R$	-
$\nu_{QPO}(0.5\text{--}10 \text{ Hz})^{(2)}$	$F_R$	- Muno et al. (2001)
$\nu_{QPO}(0.5\text{--}10 \text{ Hz})$	$T_{bb}$	+ Muno et al. (1999)

(1): direction of correlation (“+” = positive, “-” = negative),

(2): frequency of the 0.5–10 Hz QPO.

With increasing radio emission, the X-ray flux in the power law component between 20–200 keV decreases (neglecting reflection). The total 1–200 keV X-ray flux in the power law component is more or less constant. No correlation with the radio flux is seen. This is because the flux in the 1–20 keV range by far dominates, thus washing out the correlation. Muno et al. (1999) did not find a correlation of  $F_X(50\text{--}100 \text{ keV})$  with the 15 GHz radio flux. But they used a model consisting only of DISKBB and a broken power law (BKNPO) for the X-ray spectra and *RT* data with  $\pm 12$  hrs offset.

A Spearman rank-order correlation test for  $F_X(20\text{--}200)$  gives  $r_s = -0.75$ , thus showing a strong anti-correlation. For  $F_X(1\text{--}200 \text{ keV})$  the test results in  $r_s = -0.09$  and ratifies the lack of a correlation between the 1–200 keV non-thermal X-ray flux and  $F_R$ .

## 4. Discussion

Table 3 summarizes the correlations found here plus 2 relevant correlations found by Muno et al. (1999, 2000). In the following we will discuss implications of these correlations.

### 4.1. Comptonization

The origin of the hard power law component in AGN and X-ray binaries is still under discussion. Three main models exist, where the hard photons originate by inverse Compton scattering of soft disk photons on hot electrons. The main difference between these models is the distribution of the electrons. They

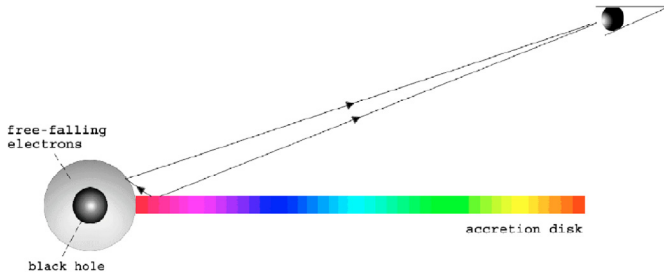


**Fig. 10.** Bulk motion geometry. Electrons become spherical free-falling between the last stable orbit and the event horizon due to shocking. The photons are comptonized on these accelerated electrons.

can be thermal (Maxwellian), non-thermal (power law like) or free falling from the last stable orbit onto the event horizon of the black hole. The high energy spectrum presents an important test for the distinction between these models. Therefore, the behavior of the power law component in GRS 1915+105 is crucial for the understanding of the electron distribution and for the geometry of the system.

It is still unclear whether or not the hard spectrum of GRS 1915+105 in the  $\chi$ -state extends with or without cutoff up to MeV energies. Due to the rapid variability of the source and the long required exposure times it is nearly impossible to get sufficiently accurate  $\gamma$ -spectra with the present high energy satellites. For example, the OSSE spectrum from 14th–20th of May 1997 reveals a power law tail up to 1 MeV without a cutoff (Iyudin 2000; Zdziarski et al. 2001). But as several contemporaneous *RXTE* observations show (which cover  $\lesssim 3\%$  of the OSSE exposure), during the observation GRS 1915+105 went through several  $\chi/\alpha$  state transitions and the PCA photon count rate from 2–40 keV varied between 5 and 25 kcts/s. Thus, the OSSE spectrum is the sum of the spectra of the  $\chi$  and  $\alpha$  (and possible other) states, with an unknown fraction coming from the  $\chi$ -state. It is therefore premature to unequivocally relate the hard MeV tail to the  $\chi$ -state.

#### 4.1.1. Bulk motion comptonization

One model for the comptonization is the bulk motion comptonization (Blandford & Payne 1981; Chakrabarti & Titarchuk 1995) (Fig. 10). The accretion stream passes the transition radius,  $r_{ts}$ , at the last stable orbit around the black hole and gets shocked. The matter falls spherical onto the event horizon. In front of the shock, the stream is similar to an optically thick, geometrically thin accretion disk (as required by the strong observed blackbody component).

The free falling electrons are accelerated up to the speed of light and inverse Compton scattering of soft photons on the electrons provides the observed power law in the hard spectrum. The model predicts a cutoff depending on the mass accretion rate (Ebisawa et al. 1996) due to inverse Compton scattering and Compton recoil. As stated above, the existence/absence of a cutoff during the  $\chi$ -states is still not secured, wherefore not statement about the model can be made from that issue.

Two major problems exist for the description of  $\chi$ -state data by the BMC model. The *RXTE* spectra of GRS 1915+105

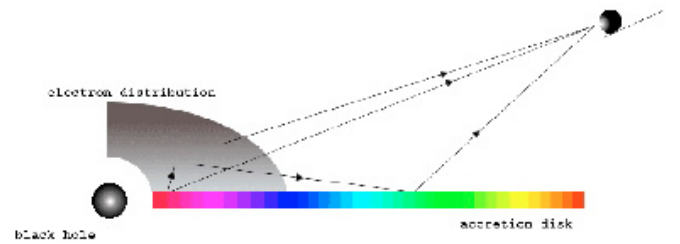


**Fig. 11.** Disk corona geometry. The disk photons are comptonized in an electron distribution located above the accretion disk. (Note, the shape and size of the electron distribution in this plot has no real physical or observational meaning.) Part of the photons are scattered back into the disk plane and are reflected or reprocessed. The photons reaching the detector are compound of the soft disk photons, the comptonized and the reflected photons.

partly show a strong reflection component. This is not compatible with the geometry of a thin disk outside a central, spherical accretion stream. The accretion stream is accelerated away from the inner disk edge onto the event horizon of the black hole. Therefore only a small part of the soft photons are comptonized back into the disk plane at  $r > r_{ts}$ . In conflict to the observations, no strong reflection component can emerge. A possible explanation for the observed reflection can then be a partly covering of the disk by an absorbing medium with  $\tau_T \sim 3$  (Zdziarski 2000). Recent Chandra X-ray spectra indeed show a high X-ray column density and abundance excesses for Si and Fe, which may be related to material that is associated with the immediate environment of the source (Lee et al. 2002).

The other problem for the BMC model is the time lag of hard and soft X-ray photons. Munro et al. (2001) found a phase lag in the 5 Hz QPO (which are connected to the hard X-ray photons) of 0.5. This corresponds to a delay of 0.1 s of the hard photons to the soft photons. The expected delay for scattering on a convergent electron stream inside  $r_{ts}$  is  $\sim 0.2$  ms, much smaller than observed. The phase lag is not constant in time and frequency and seems to vary with the radio flux.

It is obvious that the BMC model not can explain the hard power law component in the  $\chi$ -states of GRS 1915+105. There are indications that the BMC model fits other variability states. Shrader & Titarchuk (1998) found good spectral agreement of the BMC model and *RXTE* observations in the  $\rho$ -state. Note, however, that they completely neglected the time delay of hard and soft photons and the strong variability of the  $\rho$ -state for their X-ray spectral modelling.

#### 4.1.2. Thermal corona

Another possible model for the origin of the hard X-ray component is the disk corona geometry (Fig. 11) (e.g. Haardt & Maraschi 1993; Svensson & Zdziarski 1994). Soft disk photons are inverse Compton scattered on hot ( $> 20$  keV) electrons located above the disk.

Simultaneous *CGRO/OSSE* and X-ray observations of X-ray binaries with black holes showed that the high energy continuum in the low/hard state originates most likely due to thermal comptonization. The predicted cutoff in the hard X-ray spectrum is seen in Cyg X-1 (Gierliński et al. 1997), in the

**Table 4.** Fraction of the dissipated energy in the corona,  $L_{\text{diss}}$ , on the energy of the incoming photons, Compton parameter,  $y = 4\tau_{\text{T}}^2 kT_e / (m_e c^2)$  ( $\tau_{\text{T}}$  is the Thomson depth), and Compton amplification,  $A$ , for three different power law slopes.

$\Gamma$	$L_{\text{diss}}$	$y$	$A$
2.4	84%	1.33	1.84
3.0	22%	3.65	1.22
3.5	9%	7.30	1.09

LMXB GX 339-4 (Zdziarski et al. 1998) and some other X-ray transients (Grove et al. 1998).

Also the high/soft state in X-ray binaries can be explained by thermal comptonization but requires high electron temperatures in some systems to explain the observed unbroken power law up to MeV. In addition  $\tau_{\text{T}} \ll 1$  is required in order to keep the spectrum soft (Zdziarski 2000).

The power law slope is a measure of the Compton amplification,  $A(L_{\text{soft}} + L_{\text{diss}})/L_{\text{soft}}$ .  $L_{\text{diss}}$  is the dissipated energy in the corona and  $L_{\text{soft}}$  the energy of the incoming photons. Table 4 shows how  $A$  depends on  $\Gamma$  with

$$\Gamma = \frac{7}{3}(A - 1)^{-\delta} \quad (4)$$

(Beloborodov 1999) and  $\delta = 1/6$  for galactic black holes. The ratio of the dissipated energy in the corona and the energy of the intercepted soft photons gets smaller with a steeper spectrum. For the highest  $\Gamma$  only  $\sim 9\%$  of the soft photon energy is dissipated into the corona.

The minimum energy which a photon receives when passing a thermal electron distribution depends on the electron temperature  $kT_e$

$$\frac{\Delta\epsilon}{\epsilon} = \frac{4kT_e}{m_e c^2}. \quad (5)$$

The result is a lack of low energy photons when  $kT_e$  becomes large. For  $kT_e > 200$  keV the discrete orders (mainly the first) of the Compton scattering become visible as an additional peak overlaying the soft disk component. The high disk temperatures (3–4 keV) in GRS 1915+105 provide a photon deficit below 6–8 keV. This makes obvious, as already mentioned above, that a simple power law model is insufficient for the description of the comptonized photons. The lack of photons at low energies affects  $\Gamma$ ,  $K_{\text{po}}$  and the reflection component in the model.

#### 4.1.3. Hybrid corona

The radiation processes and geometry can also be described by comptonization of soft disk photons on a hybrid (thermal and non-thermal) electron distribution above an optical thick accretion disk (as in Fig. 11) (Coppi 1992). Part of the electrons in the thermal corona are accelerated, possibly in reconnection events. The disk photons are comptonized on these electrons forming the observed power law component in the hard X-ray spectrum. The energy of the non-thermal electrons is partially transferred to the thermal electrons due to Coulomb scattering. This leads to heating of the thermal electrons above the

Compton temperature. Then the thermal electrons play an important part in the up-scattering of the soft disk photons, too.

The compactness (ratio of luminosity and size) is an important parameter of the coronal plasma (Coppi 1999). A large compactness leads to electron positron pair creation due to photon photon collisions resulting in a pair annihilation line at 511 keV in the spectra. When the compactness is low, the loss of energy of the electrons due to Coulomb scattering dominates the loss due to inverse Compton scattering. The ratio of thermal to non-thermal electrons increases and the plasma becomes thermally dominated. Together with the resulting break in the distribution of the non-thermal electrons this results in a cutoff of the photon spectrum.

The rate at which non-thermal electrons appear in the hybrid electron distribution can be written as a power law (Gierliński et al. 1999)

$$\dot{N}_{\text{nt}} = \frac{dN_{\text{nt}}(\gamma)}{dt} \propto \gamma^{-\Gamma_{\text{in}}}. \quad (6)$$

Here,  $\gamma$  is the Lorentz factor of the non-thermal electrons and  $\Gamma_{\text{in}}$  the power law slope of the injected soft photon distribution, which influences the slope of the power law spectrum as

$$\Gamma_{\text{in}} \simeq 2(\Gamma - 1). \quad (7)$$

The observed power law slope  $\Gamma \sim 2.5$  ( $\Gamma \sim 3.5$ ) implies  $\dot{N}_{\text{nt}} \propto \gamma^{-3}$  ( $\propto \gamma^{-5}$ ). Therefore the fraction of non-thermal electrons decreases with steepening power law.

In GRS 1915+105, the observed continuous distribution of  $\Gamma$  between 2.4 and 3.5 is evidence for a variability in the power law component and thus in the composition and locus of the electron distribution. From the observation of the reflection and the 0.5–10 Hz QPO it is conspicuous that the electron distribution must have a small (relative to the system) spatial size. As a small compactness, e.g. large plasma volume, results in a spectral cutoff, for the  $\chi$ -states of GRS 1915+105 a hybrid electron distribution not can be ruled out. It is difficult to distinguish spectroscopically between a hybrid and a thermal plasma if the hybrid plasma is thermally dominated. The only possibility is the search for the predicted photon excess at high energies and for the annihilation line (Coppi 1999). For a better understanding, enhanced high energy detectors, such as on INTEGRAL, are required. The analysis of such spectra also needs further developed physical models, instead of a simple power law.

The investigation of the *RXTE* data of GRS 1915+105 with the DISKBB+REFSCH model does not allow a definite conclusion about the origin of the hard spectral component. Only the BMC model is ruled out for the  $\chi$ -states. Though a clear distinction between a thermal and a hybrid not can be proposed, it seems clear that the thermal electrons dominate.

It has been shown above (Fig. 5) that two different states of comptonization with two different pivoting energies are observed. Very recently (Zdziarski et al. 2002) pivoting was found also in Cyg X-1. A varying amount of soft seed photons undergoing the comptonization process probably accounts for the pivoting of the spectrum. One possible explanation is a constant disk blackbody and an expanding/contracting hot coronal plasma. A change in the size of the corona leads to a change

in the fraction of intercepted soft photons. Assuming constant optical plasma depth,  $\tau_T$ , if the soft luminosity is high, the electrons in the corona are cooled efficiently and the spectrum of the comptonized photons is soft. On the other hand, if the soft luminosity decreases, the temperature of the corona increases and the spectrum hardens). The occurrence of two differing pivoting branches suggests the existence of two states with different  $\tau_T$  and/or different electron composition (thermal/non-thermal).

#### 4.2. Reflection

The reflection of X-rays on an accretion disk manifests itself in two specific spectral features: (i) the characteristic emission line spectrum (mainly the  $K\alpha$  lines of the most common metals) with the 6.4 keV iron emission lines as the strongest and (ii) a characteristic hump arises above 10 keV because of the energy dependence of the cross section of absorption and Compton scattering.

Observations with *ASCA* in different variability states indicate a variable iron absorption or emission in GRS 1915+105 (Ebisawa et al. 1997). The iron emission at 6.4 keV dominates the spectra from 25.10.1996 and 25.04.1997 whereas a distinct absorption at 7 keV and no emission was seen on 27.09.1994 and 26.04.1995. During the 25.04.1997 observation GRS 1915+105 switched between  $\chi$ - and  $\alpha$ -states (based on *RXTE* data). Therefore, it is not clear whether the emission line originates during the  $\chi$ - or during the  $\alpha$ -interval. No statement can be made about the states during the other *ASCA* observations due to lack of corresponding *RXTE* observations.

Recent *Chandra* data of GRS 1915+105 obtained in the low hard state revealed neutral K absorption edges, ionized resonance absorption from Fe (XXV, XXVI) and possible emission from neutral Fe  $K\alpha$  and ionized Fe XXV (Lee et al. 2002), suggesting conditions favorable for reflection.

##### 4.2.1. Reflection in LMXB and AGN

Investigations of Seyfert galaxies and X-ray binaries in the low/hard state show a correlation between the slope of the hard X-ray component and the reflection. Incoming radiation with a steeper slope is more reflected than radiation with a flatter slope.

The reflection is stronger in black hole candidates than in Seyfert galaxies for a given  $\Gamma$  (Zdziarski 1999). This can be explained using an optical thick accretion disk. The different masses of the black holes imply different maximum energies of the blackbody photons (Svensson 1996). The hard X-ray photons from the corona can ionize the upper layers of the accretion disk and an ionized layer above neutral matter evolves. If  $\Gamma$  is large the heating of the disk is small and the cold layer of the disk lies near the disk surface. With decreasing power law slope the temperature of the upper layer and therefore the ionization increases, the absorption is smaller, more photons are scattered and the characteristic reflection hump is suppressed, sufficient to explain the observed  $R(\Gamma)$ -correlation.

The correlation in Seyfert galaxies is generally steeper than that observed in X-ray binaries (Zdziarski 1999). In Seyferts the correlation has been explained with a model consisting of a static, thermal corona above a neutral reflector (Svensson 1996). The existence of the  $R(\Gamma)$ -correlation implies a feedback where the existence of the reflecting matter influences the hardness of the X-ray spectrum (Böttcher et al. 1998; Zdziarski et al. 1999). Assuming that the cold matter (the accretion disk) emits soft photons which become seed photons of the comptonization, than with increasing solid angle of the reflector (here the accretion disk) the flux of soft photons increases and the cooling rate of the hot corona increases. For a thermal plasma the resulting power law component steepens with increasing cooling rate.

On the other hand, models which are based on non-thermal electrons should not show a dependence of spectral hardness and cooling rate (Lightman & Zdziarski 1987; Zdziarski et al. 1999). Models in which the seed photons are intrinsically produced in the hot plasma (e.g. synchrotron radiation) not can reproduce the observed correlation. The power law slope is then independent of the reflection.

##### 4.2.2. Reflection in GRS 1915+105

The  $\chi$ -states in GRS 1915+105 show a similar correlation as seen in Seyfert galaxies and X-ray binaries (Zdziarski et al. 1999). The reflection amplitude is strongly effected by the disk model. The higher the disk temperature, the larger the reflection amplitude. The disk temperatures in X-ray binaries are higher than in Seyfert galaxies. In GRS 1915+105 the temperature of the disk is still higher, explaining why a majority of the GRS 1915+105 data lies above the correlation function (showing slightly higher  $R$  for a given  $\Gamma$ ) in Fig. 7.

The reflection amplitude of  $R > 1$  strongly suggests an anisotropic inverse Compton process. The dominant fraction of the up-scattered soft disk photons is directed back into the plane of the accretion disk. This produces the observed large reflection amplitude in contrast to an isotropic scattering where  $R \leq 1$ .

Observations of GRS 1915+105 show a strongly varying  $\Gamma$ , therefore the corona can hardly be static above the reflector. In GRS 1915+105,  $\Gamma$  increases with increasing radio emission. Higher radio emission may imply more outflow away from the disk with  $\beta = (v/c) > 0$ . Thus, the higher the mass outflow, the lower the electron temperature which is required to produce the observed amount of comptonization. On the other hand, with a dynamical, thermal corona the spectrum hardens with increasing  $\beta$  due to relativistic aberration, giving a flatter power law with higher outflow velocity (Malzac et al. 2001).

The observation in GRS 1915+105 predicts an at least partly thermal source of the hard X-ray photons and an important contribution of the cooling due to the soft photons. This allows both a thermal and a hybrid electron distribution.

It is more difficult to interpret the behavior of observations with high  $\Gamma$  and small  $R$  in Fig. 7. Unlike in a thermal plasma, the Compton scattering in a non-thermal plasma does not depend on the cooling rate of the soft photons, instead it depends

on the slope of the electron distribution (Poutanen & Coppi 1998). A change in the properties of the plasma can provide the differing behavior.

For a better determination of the correlation and for conclusions about the distinct system components, more complex ionization models are needed. They partly exist (Done & Nayakshin 2000) but require too much computing power to be useful for the analysis of real spectra at this stage.

### 4.3. X-ray-radio-correlation

The lack of a correlation of the radio flux with any of the disk parameters is somewhat unexpected since the (short-duration) low/hard states have earlier been related to jet ejections with radio emission by synchrotron radiation of the ejected plasma (Pooley & Fender 1997). Since IR (Eikenberry et al. 2000) and radio observations (Pooley & Fender 1997; Fender & Pooley 2000) have led to the conclusion that GRS 1915+105 shows jets on various scales, or even has a continuous distribution of jet strength, one would have expected that also in  $\chi$ -states the radio flux correlates with the disk temperature/emissivity.

The matter in the sporadic, relativistic jets may originate from disruption of the inner part of the accretion disk during  $\beta$ -states (Mirabel et al. 1998). In  $\chi$ -states no correlation of the radio emission and the inner disk radius is observed. Instead, the hard spectral component is correlated with the radio flux.

Muno et al. (1999) found a positive correlation of the accretion disk temperature and the frequency of the 0.5–10 Hz quasi periodic oscillations, and of the radio flux with the QPO frequency (Muno et al. 2001). With increasing  $T_{\text{bb}}$  and decreasing radio emission the QPO frequency increases. This predicts a negative correlation of  $T_{\text{bb}}$  and radio flux. The fact that nothing like this is found in the present analysis can have several reasons. As mentioned before, Muno et al. (1999) used the standard model DISKBB+BKNPO for the analysis of the *RXTE* spectra. This seems not suitable for the  $\chi$ -states of GRS 1915+105. Accordingly, the disk temperature and therefore the correlation of the QPO frequency and the disk temperature have to be interpreted carefully.

It is generally assumed that both the radio jets (Fendt & Greiner 2001; Fender 2001) and the hard spectral component originate near the black hole. With increasing outflow of matter (therefore increasing radio emission) the interaction with the electron distribution becomes significant. Similar to the interpretation of the pivoting behavior of the X-ray spectra, an increasing outflow of matter implies an increasing size of the scattering medium and therefore an increasing amount of intercepted soft seed photons. This leads to a lower plasma temperature due to cooling and to a softer X-ray spectrum, which is seen in the  $\Gamma(F_{\text{R}})$ -correlation. Simultaneously, the outflowing matter intermingles with the coronal matter and pushes it away from the accretion disk. The formerly thermally dominated electron distribution may become non-thermal dominated. This should result in a shift of the cutoff of the power law component in the  $\chi$ -states with higher radio emission above the HEXTE range to higher energies.

When the radio emission is low, the observed power law is supposed to originate in the corona above the accretion disk. Assuming that the radio quiet state lacks outflow of matter or the effect of the outflow on the corona is negligible, the hard spectral component possibly originates due to comptonization of disk photons in the corona. A thermal electron distribution can then explain the X-ray spectra of the radio quiet  $\chi$ -states.

The hard X-ray component in  $\chi$ -states therefore comes most likely from soft disk photons which are inversely scattered on a thermal dominated electron distribution (when radio flux is low) or on the base of a continuous jet (when radio flux increases). The suggestion of the base of the jet as source of the hard X-ray photons was already made by Fender (2001). Only the increasing reflection with increasing radio flux is still unresolved.

In conflict with the anti-correlation of  $F_{\text{X}}(20\text{--}200)$  and  $F_{\text{R}}$  in GRS 1915+105 a linear correlation is observed on the LMXB GX 339-4 (Corbel et al. 2000). With increasing radio flux the X-ray flux increases. This is true for the hard (20–100 keV) and for the soft X-ray flux (2–12 keV) where GRS 1915+105 shows no correlation. The soft disk component in GX 339-4 is negligible above 2 keV and the power law component alone quantifies the flux. Although GRS 1915+105 shows an equal  $R(\Gamma)$ -correlation as GX 339-4 the  $\Gamma(F_{\text{R}})$ - and  $F_{\text{X}}(F_{\text{R}})$ -correlation is opposite. That is remarkable because the  $R(\Gamma)$ -correlation suggests a similar structure near the black hole (especially the corona) in GRS 1915+105 and GX 339-4. No such correlation of  $F_{\text{X}}$  and  $F_{\text{R}}$  is observed in Cyg X-1 (Brocksopp et al. 1999).

In principle the hard X-ray photons can originate in the continuous jet itself. But following the equations of Marscher (1983) the hard X-ray photons from self comptonization of a compact synchrotron jet are negligible with regard to the coronal contribution. An analogous result was found for Cyg X-1 and GX 339-4. The contribution of thermal X-ray bremsstrahlung in the jet is also too small to explain the observed hard X-ray luminosities (Memola et al. 2002).

## 5. Conclusion

The analysis of 139 *RXTE* observations of GRS 1915+105 in the  $\chi$ -state revealed variable components and parameters of the X-ray spectra. The structure of the hard X-ray power law depends e.g. on the radio flux. Further, a two-branch correlation of the power law slope and the power law normalization was found. These branches show different pivoting behavior.

The most probable geometry is that of a hot corona above the accretion disk. A bulk motion comptonization seems to be ruled out for the  $\chi$ -states because of the time lags of hard and soft X-ray photons.

The continuous outflow of matter is not correlated with the accretion disk parameters as measured at X-rays. Neither the disk temperature nor the inner disk radius are connected with the radio flux. Therefore, the outflowing matter should not be provided by a disruption of the inner part of the accretion disk, as thought to be the case for the sporadic jets in GRS 1915+105, and a positive correlation between radio emission and power law slope is found. Because both the base of the

jet and the corona are probably located near the black hole the correlation indicates an interaction of both structures. Whereas during low radio emission the hard X-ray component originates due to comptonization on a thermally-dominated corona, in radio loud states the comptonization should appear in the out-flowing matter.

GRS 1915+105 shows a positive  $R(\Gamma)$ -correlation as seen in other X-ray binaries and AGN. The large reflection amplitude suggests a highly anisotropic inverse Compton scattering with the dominant part of the soft photons being scattered back into the disk plane.

*Acknowledgements.* The authors thank E. H. Morgan (MIT) and G. G. Pooley (MRAO) for providing the ASM and *RT* data and W. A. Heindl (*RXTE*) and K. A. Arnaud (*XSPEC*) for their comments. We thank the referee, A. Zdziarski, for the thorough reading and several suggestions which improved the presentation and T. Belloni for the constructive criticism. The *Ryle Telescope* is supported by PPARC. The *Green Bank Interferometer* is a facility of the National Science Foundation operated by the NRAO in support of NASA High Energy Astrophysics programs.

## References

- Arnaud, K. A. 1996, in *Astronomical Data Analysis Software and Systems*, ed. G. H. Jacoby, & J. Barnes, ASP Conf. Ser., 101, 17
- Balucinska-Church, M., & McCammon, D. 1992, *ApJ*, 400, 699
- Belloni, T., Mendez, M., King, A. R., van der Klis, M., & van Paradijs, J. 1997, *ApJ*, 488, L109
- Belloni, T., Klein-Wolt, M., Mendez, M., van der Klis, M., & van Paradijs, J. 2000, *A&A*, 355, 271
- Beloborodov, A. M. 1999, in *High Energy Processes in Accreting Black Holes*, ed. J. Poutanen, & R. Svensson, ASP Conf. Ser., 161, 295
- Blandford, R. D., & Payne, D. G. 1981, *MNRAS*, 194, 1041
- Böttcher, M., Liang, E. P., & Smith, I. A. 1998, *A&A*, 339, 87
- Brocksopp, C., Fender, R. P., Larionov, V., et al. 1999, *MNRAS*, 309, 1063
- Castro-Tirado, A.J., Brandt, S., & Lund, N. 1992, *IAU, Circ.*, 5590
- Chakrabarti, S. K., & Titarchuk, L. G. 1995, *ApJ*, 455, 623
- Chaty, S., Mirabel, I. F., Duc, P. A., Wink, J. E., & Rodriguez, L. F. 1996, in *Proc. Roentgenstrahlung from the Universe*, ed. H. U. Zimmermann, J. Trümper, & H. Yorke, MPE Report, 263, 129
- Corbel, S., Fender, R. P., Tzioumis, A. K., et al. 2000, *A&A*, 359, 251
- Coppi, P. S. 1992, *MNRAS*, 258, 657
- Coppi, P. S. 1999, in *High Energy Processes in Accreting Black Holes*, ed. J. Poutanen, & R. Svensson, ASP Conf. Ser., 161, 375
- Done, C., & Nayakshin, S. 2000, *ApJ*, 546, 419
- Ebisawa, K., Titarchuk, L. G., & Chakrabarti, S. K. 1996, *PASJ*, 48, 59
- 97 Ebisawa, K., Takeshima, T., White, N. E., et al. 1997, poster contribution of IAU Symp., 188  
<ftp://lheaftp.gsfc.nasa.gov/pub/ebisawa/kyoto.ps.gz>
- Eikenberry, S. S., Matthews, K., Muno, M., et al. 2000, *ApJ*, 532, L33
- Fabian, A. C., Rees, M. J., Stella, L., & White, N. E. 1989, *MNRAS*, 238, 729
- Fender, R. P., Bell Burnell, S. J., Garrington, S. T., Spencer, R. E., & Pooley, G. G. 1995, *MNRAS*, 274, 633
- Fender, R. P., & Pooley, G. G. 2000, *MNRAS*, 318, L1
- Fender, R. P. 2001, in *Black Holes in Binaries and Galactic Nuclei*, ed. L. Kopper, E. P. J. van den Heuvel, & P. A. Woudt, 193
- Fendt, C., & Greiner, J. 2001, *A&A*, 369, 308
- Gierliński, M., Zdziarski, A. A., Done, C., et al. 1997, *MNRAS*, 288, 958
- Gierliński, M., Zdziarski, A. A., Poutanen, J., et al. 1999, *MNRAS*, 309, 496
- Gilfanov, M., Churazov, E., & Revnitsev, M. 2000, in *Proc. of the 5th CAS/MPG Workshop on High Energy Astrophysics*, ed. G. Zhao et al. (Beijing: China Sci. Tech. Press), 114
- Greiner, J., Snowden, S., Harmon, B.A., Kouveliotou, C., & Paciesas, W. 1994, 2nd Compton Symp., AIP, 304, 260
- Greiner, J., Morgan, E. H., & Remillard, R. A. 1996, *ApJ*, 473, L107
- Greiner, J., Cuby, J. G., McCaughrean, M. J., Castro-Tirado, A. J., & Mennickent, R. E. 2001a, *A&A*, 373, 37
- Greiner, J., Cuby, J. G., & McCaughrean, M. J. 2001b, *Nature*, 414, 522
- Grove, J. E., Johnson, W. N., Kroeger, R. A., McNaron-Brown, K., & Skibo, J. G. 1998, *ApJ*, 500, 899
- Haardt, F., & Maraschi, L. 1993, *ApJ*, 413, 507
- Iyudin, A. F. 2000, *Nucl. Phys. B*, 85, 263
- Jahoda, K., Swank, J. H., Giles, A. B., et al. 1996, *Proc. SPIE*, 2808, 59
- Kotani, T., Ebisawa, K., Dotani, T., et al. 2000, *ApJ*, 539, 413
- Lee, J. C., Reynolds, C. S., Remillard, R. A., et al. 2002, *ApJ*, 567, 1102
- Lightman, A. P., & Zdziarski, A. A. 1987, *ApJ*, 319, 643
- Magdziarz, P., & Zdziarski, A. A. 1995, *MNRAS*, 273, 837
- Malzac, J., Beloborodov, A. M., & Poutanen, J. 2001, *MNRAS*, 326, 417
- Marscher, A. P. 1983, *ApJ*, 264, 296
- Marti, J., Mirabel, I. F., Chaty, S., & Rodriguez, L. F. 2000, *A&A*, 356, 943
- Memola, E., Fendt, C., & Brinkman, W. 2002, *A&A*, 385, 1089
- Mirabel, I. F., Rodriguez, L. F., Cordier, B., Paul, J., & Lebrun, F. 1992, *Nature*, 358, 215
- Mirabel, I. F., & Rodriguez, L. F. 1994, *Nature*, 371, 46
- Mirabel, I. F., Bandyopadhyay, R., Charles, P. A., Shabaz, T., & Rodriguez, L. F. 1997, *ApJ*, 477, L45
- Mirabel, I. F., Dhawan, V., Chaty, S., et al. 1998, *A&A*, 330, L9
- Morgan, E. H., Remillard, R. A., & Greiner, J. 1997, *ApJ*, 482, 993
- Muno, M. P., Morgan E. H., & Remillard, R. A. 1999, *ApJ*, 527, 321
- Muno, M. P., Remillard, R. A., Morgan, E. H., et al. 2001, *ApJ*, 556, 515
- Orosz, J. A., & Bailyn, C. D. 1997, *ApJ*, 477, 876
- Pooley, G. G., & Fender, R. P. 1997, *MNRAS*, 292, 925
- Poutanen, J., & Coppi, P. S. 1998, *Phys. Scr.*, T77, 57
- Press, H. W., Teukolsky, S. A., Vetterling, W. T., & Flannery, B. P. 1992, *Numerical Recipes* (Cambridge)
- Shrader, C., & Titarchuk, L. G. 1998, *ApJ*, 499, L31
- Svensson, R., & Zdziarski, A. A. 1994, *ApJ*, 436, 599
- Svensson, R. 1996, *A&AS*, 120, 475
- Trudolyubov, S. P. 2001, *ApJ*, 558, 276
- Vilhu, O., Poutanen, J., Nikula, P., & Nevalainen, J. 2001, *ApJ*, 533, L51
- Zdziarski, A. A., Poutanen, J., Mikołajewska, J., et al. 1998, *MNRAS*, 301, 435
- Zdziarski, A. A. 1999, in *High Energy Processes in Accreting Black Holes*, ed. J. Poutanen, & R. Svensson, ASP Conf. Ser., 161, 16
- Zdziarski, A. A., Lubinski, P., & Smith, D. A. 1999, *MNRAS*, 3030, L11
- Zdziarski, A. A. 2000, in *Highly Energetic Physical Processes and Mechanisms for Emission from Astrophysical Plasmas*, IAU Symp., 195, 153
- Zdziarski, A. A., Grove, J. E., Poutanen, J., Rao, A. R., & Vadawale, S. V. 2001, *ApJ*, 554, L45
- Zdziarski, A. A., Poutanen, J., Paciesas, W. S., & Wen, L. 2002, *ApJ*, in press [[astro-ph/0204135](mailto:astro-ph/0204135)]